



Contents lists available at ScienceDirect

Arabian Journal of Chemistry

journal homepage: [www.sciencedirect.com](http://www.sciencedirect.com)

Original article

## MIL-101 (Cr) hybrid nanoporous carbon derived MOF as a nano-adsorbent for dye removal using RSM-CCD

Soheila Sharafinia<sup>a</sup>, Alimorad Rashidi<sup>b,\*</sup><sup>a</sup> Department of chemistry, Faculty of Science, Shahid Chamran University of Ahvaz, Ahvaz, Iran<sup>b</sup> Nanotechnology Research Center, Research Institute of Petroleum Industry (RIPI), Tehran, Iran

## ARTICLE INFO

## Article history:

Received 5 March 2023

Accepted 20 September 2023

Available online 26 September 2023

## Keywords:

MIL-101 (Cr)

MOF-5

RSM-CCD

Nanoporous Carbon

Methylene Blue

Metal-organic Framework

## ABSTRACT

Metal-organic frameworks (MOFs) are a promising class of nanoporous crystalline materials with potential applications in gas storage, catalysis, biomedical, adsorption, and clean energy. The massive parts of commercial dyes are interfering to our environment and are considered danger for humans and animals. In this research work, nanohybrids based on MOFs have been studied as a suitable nanoadsorbent for the adsorption of cationic dyes such as methylene blue (MB). In this article, a nanopore carbon (NPC) was prepared from Zn-MOF. The Zn-MOF NPC with MI-101 NPs has been used to prepare Zn-MOF NPC@MIL nanohybrid by the hydrothermal method. Various XRD, FT-IR, SEM, EDX, TEM, TGA, and BET techniques have been used to characterize the nano adsorbent. Four essential variables effective in adsorption, loading percentage of NPs, initial concentration of MB, contact time and pH, were optimized by Central Composite Response Surface Method (RSM-CCD). The removal percentage (Re%) of MB is equal to 95.7% was obtained under the following conditions: The loading value of 25Wt.%, the MB initial concentration of 50 mg. L<sup>-1</sup>, contact time 30 min and pH 8. Also, the experimental data were investigated with famous kinetic models and isotherms, and it was observed that MB removal by nanohybrid is correlated with pseudo-second-order kinetic model and Langmuir isotherm.

© 2023 The Author(s). Published by Elsevier B.V. on behalf of King Saud University. This is an open access article under the CC BY-NC-ND license (<http://creativecommons.org/licenses/by-nc-nd/4.0/>).

## 1. Introduction

With the increasing population growth and the needing for humans in the development of industry, major toxic compounds have entered the water, and caused change in the water quality, therefore it endangers the life of living beings and the environment. One of the toxic compounds are dyes, which have a wide range in the textile, leather, food, plastic and paper industries (Tanhaei et al., 2019). About 4–5 % of azo dyes are dangerous, and most of them have disadvantages such as high toxicity, complex aromatic structure, high resistance to degradation (Liu et al., 2014), and non-biodegradability. Most of these dyes can cause diseases such as mental retardation, deformity, and cancer (Xu et al., 2019). Therefore, it is necessary to remove these pollutants from water sources. There are various methods, including chemical ox-

idation/reduction (Rahmaninia et al., 2019; Babaei et al., 2018; Bezaatpour et al., 2017), ion exchange, physical adsorption, and membrane filtration, for the treatment of dye-related wastewater (Liu et al., 2015). In recent years, the adsorption method has widely attracted the attention of many researchers in the wastewater treatment. The adsorption process has advantages such as easy study, high efficiency, high capacity, and cost-effectiveness (Liu et al., 2012).

The adsorption process is an excellent method able to detect and adsorption simultaneously. This method has distinguished advantages as follows:

- 1) Simplicity of detection and adsorption processes (Liu et al., 2012).
- 2) Significant reduction of consumption costs (Chen et al., 2017).
- 3) Increase in the detection capability of the substance due to the initial enrichment of the adsorption process (Seenivasan et al., 2015).

Therefore, the simultaneous adsorption and detection strategy is fully compatible with the severe environmental regulatory requirements. Recently, different substances such as metal oxides (Macdonald and Veinot, 2008), magnetic nanoparticles (NPs) (Luo et al., 2016), polymers (Wang et al., 2017), Ag-doped ZnO (Azizian, 2004); and graphene-based materials (Kong et al., 2017)

\* Corresponding author.

E-mail address: [rashidiam@ripi.ir](mailto:rashidiam@ripi.ir) (A. Rashidi).

Peer review under responsibility of King Saud University.



Production and hosting by Elsevier

have been used to remove of these pollutants. Nevertheless, the manufacture of these sorbents is very time-consuming, and they have low surface area (Zhang et al., 2012), which reduced the efficiency of the adsorption process.

Metal-organic frameworks (MOFs) are a new generation of materials that have achieved high surface area by forming multidimensional structures (one, two, or three dimensions) (Farha and Hupp, 2010).

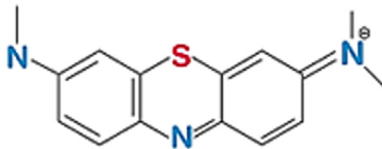
In recent years, most MOFs have attracted the attention of researchers in many fields, such as heavy metal ions adsorption (Abney et al., 2014), dyes removal (Farha et al., 2010), gas adsorption (Li et al., 2014), separation (Horcajada et al., 2010), catalysis, and drug delivery (Zhou et al., 2021), due to their diversity in composition and structure, high thermal and chemical stability, and the ability to adjust porosity (by changing organic linkers). In addition, their functions and structures can be adjusted for requested applications (O'Keeffe and Yaghi, 2012).

Nanoporous carbons (NPCs) have excellent potential as substances of adsorbent, gas storage, electrodes, and catalyst support, due to fast kinetics, high porosity and surface area (Kaneti et al., 2017; Salunkhe et al., 2016; Szczyński et al., 2018). NPCs are prepared by various methods such as physical or chemical activation (Ahmadpour and Do, 1996), templating (Yang et al., 2005; Liu et al., 2010); chemical vapor deposition (CVD) (Liu et al., 2010), electric arc (Journet et al., 1997), and laser ablation (Liu et al., 2010). So far, various MOFs ( $\text{Cu}_3(\text{BTC})_2$ ) (Wang et al., 2018), MIL-53 (Marpaung et al., 2019), UiO-66 (Cabello et al., 2018), MOF-199 (XXu et al., 2017), ZIF-67 (Lin and Chen, 2016), ZIF-8 (Torad et al., 2013), and MOF-5 (Li et al., 2018) have been used as precursors for the synthesis of NPCs with uniform particle shape and size. One of the important factors in determining the structure of the resulting materials is the wise selection of precursors (i.e. MOFs). MOF-5 is a famous and three-dimensional framework based on Zn metal and 1, 4-benzene dicarboxylic acid ( $\text{H}_2\text{BDC}$ ) linker (Yuan et al., 2009).

In this work, MOF-5 was used as a precursor for preparation, and then NPCs were assembled by direct carbonization of MOF-5. Subsequently, the resulting NPCs were hybridized with MIL-101 (Cr) ( $\text{Cr}_3\text{F}(\text{H}_2\text{O})_2\text{O}[(\text{O}_2\text{C})-\text{C}_6\text{H}_4-(\text{CO}_2)]_3 \cdot n\text{H}_2\text{O}$ ) to increase the surface area, increase the physical/chemical stability, and improve the adsorption efficiency, and finally were used to remove the methylene blue (MB) cationic dye (see Table 1).

MIL-101 (Cr) is a very attractive MOF due to its large surface area, abundant nanoscale cavities (mesoporous cages (29 and 34 Å) accessible through microporous windows (12 Å and 14 Å),

**Table 1**  
The physicochemical properties of the MB.

Molecular structure	
3D model structure	
Molecular formula	$\text{C}_{16}\text{H}_{18}\text{N}_3\text{S}^+$
Molecular weight ( $\text{g}\cdot\text{mol}^{-1}$ )	284.4
$\lambda_{\text{max}}$ (nm)	664

and high adsorption performance (Salehi and Hosseini, 2021). The Zn-MOF NPC@MIL has indicated excellent adsorption  $\text{Re}\%$  to the adsorption of MB molecules (95.7%), which is a significant value compared to other reported adsorbents. Also, the results of the experiments were analyzed using Design-Expert software, and the optimum parameters (pH, contact time, initial concentration of MB, the loading percentage of MIL-101 (Cr) on Zn-MOF NPC) were used to study the thermodynamics and kinetics of the reactions. The results showed that the experimental data corresponded with the pseudo-quadratic kinetic model Langmuir isotherm.

## 2. Experimental section

### 2.1. Materials

The chemicals used in this research work were purchased from Merck (Darmstadt, Germany) as follows: Zinc nitrate hexahydrate ( $\text{Zn}(\text{NO}_3)_2 \cdot 6\text{H}_2\text{O}$ ),  $\text{H}_2\text{BDC}$ , Chromium nitrate nonahydrate ( $\text{Cr}(\text{NO}_3)_3 \cdot 9\text{H}_2\text{O}$ ), ammonium fluoride ( $\text{NH}_4\text{F}$ ), absolute methanol (MeOH), absolute N, N-dimethylformamide (DMF), absolute hydrofluoric acid (HF).

### 2.2. Fabrication of Zn-MOF-5 NPC

The Zn-MOF-5 NPC was prepared through the direct carbonization of Zn-MOF-5 as presented in the work of Wang et al. (Jiao et al., 2016). Briefly, 10.4 g of  $\text{Zn}(\text{NO}_3)_2 \cdot 6\text{H}_2\text{O}$ , 2 g of  $\text{H}_2\text{BDC}$ , and 70 ml of DMF were added to a 250 ml flask and stirred to completely dissolve the solids. Then the mixture was heated under reflux at 120 °C for 24 h. After cooling the mixture to room temperature, the resulting white precipitate was separated by centrifuge (9000 rpm and 10 min), and washed three times with DMF. Then the Zn-MOF-5 NPs were immersed in fresh chloroform for 12 h and finally dried in a vacuum oven under a 60 °C for 12 h. In the calcination stage, the Zn-MOF-5 powders obtained from the previous step were placed in a ceramic crucible, then was transferred to a furnace under a nitrogen atmosphere. The temperature was increased at a rate of 5 °C  $\text{min}^{-1}$ , and calcined at 900 °C for 6 h (Fig. 1A).

### 2.3. Fabrication of Zn-MOF-5 NPC@MIL nanohybrid

MIL-101 (Cr) NPs were synthesized by hydrothermal method (Férey et al., 2005), 1 g of Zn-MOF NPC, 8 g of  $\text{Cr}(\text{NO}_3)_3 \cdot 9\text{H}_2\text{O}$  and 3.32 g of  $\text{H}_2\text{BDC}$  were added to 96 ml of distilled water and stirred for 20 min. Then, 20 mmol of HF was added to the mixture and it was vigorously stirred for another 20 min. The resulting suspension was transferred to the autoclave and kept in the oven for 24 h at 220 °C. The obtained green product was cooled to room temperature and centrifuged for the washing process (Fig. 1B).

### 2.4. Post-synthesis and purification

In order to purify the Zn-MOF-5 NPC@MIL nanohybrid samples from unreacted  $\text{H}_2\text{BDC}$  species, the sample was washed as follows:

Initially, the powders were washed three times with DMF (80 °C) and five times with distilled water (100 °C) and centrifuged. Then the samples were refluxed for 8 h in DMF at 80 °C and separated by centrifuge after cooling. The resulting product was soaked in MeOH for four days at 25 °C (Note: MeOH was regularly changed every day). After that, the powders were activated in a vacuum oven at 140 °C for 12 h. Finally, to remove the residual  $\text{H}_2\text{BDC}$ , the samples were stirred in  $\text{NH}_4\text{F}$  aqueous solution at 65 °C for 5 h ( $\text{NH}_4\text{F}$  amount: 100  $\text{cm}^3$  of 30 mM solution per 1 g of dried powder in the previous step). To remove any remaining  $\text{NH}_4\text{F}$

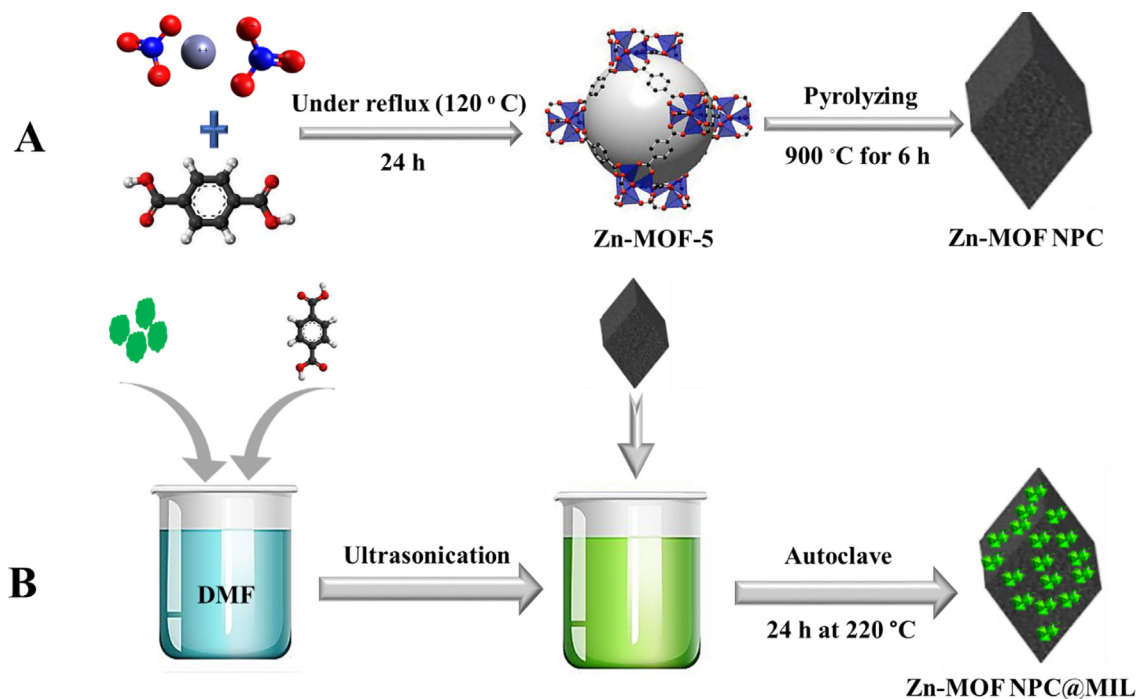


Fig. 1. Schematic image of A) Zn-MOF NPC, B) Zn-MOF NPC@MIL nanohybrid synthesis.

molecules inside the pores, Zn-MOF-5 NPC@MIL nanohybrids were washed three times with distilled water (100 °C) and centrifuged. The obtained Zn-MOF-5 NPC@MIL nanohybrid was activated for 12 h in a vacuum oven at a 140 °C. The prepared product is denoted as Zn-MOF-5 NPC@MIL 10 % nanohybrid. The preparation of other sorbents of A (15--30 %) was carried out with this method but with different amounts of Zn and H<sub>2</sub>BDC.

### 2.5. Batch adsorption experiments

A stock solution with a concentration of 200 ppm MB was prepared and then diluted to prepare a dye solution with a concentration of 20–140 ppm. Also, a shaker incubator (175 rpm) was used to perform adsorption tests under experimental conditions. The Re% and the equilibrium adsorption capacity ( $q_e$ , mg. g<sup>-1</sup>) of MB in the designed experimental conditions were calculated from Eqs. 1 and 2, respectively.

$$Re\% = \frac{C_0 - C_e}{C_0} \times 10 \quad (1)$$

$$q_e = \frac{(C_0 - C_e)V}{W} \quad (2)$$

Where in these relations  $C_0$  (mg. L<sup>-1</sup>),  $C_e$  (mg. L<sup>-1</sup>), V, and W are represented the initial concentration, equilibrium concentration, the volume of the MB solution (L), and the adsorbent weight (g) (Yagub et al., 2014).

## 3. Results and discussion

FT-IR spectroscopy was used for the characterization of surface functional groups of Zn-MOF NPC, MIL-101 (Cr), and Zn-MOF NPC@MIL nanohybrids (Fig. 2A). As can be seen, in the spectrum of the Zn-MOF NPC sample, many peaks have been removed or reduced in intensity compared to the Zn-MOF sample. This confirms that many functional groups in Zn-MOF have disappeared due to the carbonization process. Peaks corresponding to N–H or O–H stretching modes of the amine and hydroxyl groups appeared

at 3400 cm<sup>-1</sup> (Ma et al., 2018; Zhao et al., 2015). Also, the peaks of 1625 cm<sup>-1</sup>, 1152 cm<sup>-1</sup>, and 1090 cm<sup>-1</sup> correspond to the C = C stretching vibration of the aromatic rings, C–O and C–C stretching vibrations, respectively (Ma et al., 2018; Chang et al., 2015). A study of the spectrum of the MIL-101 (Cr) NPs confirmed the existence of a strong peak related to the stretching vibration of Cr–O at 570 cm<sup>-1</sup>. On the other hand, many peaks observed in the 600–1600 cm<sup>-1</sup> are assigned to the aromatic rings of the H<sub>2</sub>BDC linker. For example, the peaks related to the vibration of the C–H group in CH<sub>3</sub> have appeared in the 750 cm<sup>-1</sup>, 884 cm<sup>-1</sup>, 1017 cm<sup>-1</sup>, and 1160 cm<sup>-1</sup>, and the peak in the region of 1508 cm<sup>-1</sup> is due to the stretching C = C double bond. A sharp peak at 1404 cm<sup>-1</sup> confirms the formation of dicarboxylate in the MIL-101 (Cr) structure, which is related to O–C–O symmetric stretching. The vibrational bands appearing at 1625 cm<sup>-1</sup> and 3400 cm<sup>-1</sup> indicate the presence of adsorbed water. Furthermore, the weak peak at 1669 cm<sup>-1</sup> signaled the existence of negligible unreacted H<sub>2</sub>BDC linker in the pores, and therefore the success of purification and post-treatment process. Hence, the appearance of these peaks in the Zn-MOF NPC@ MIL nanohybrid provides a strong evidence for the formation of Zn-MOF NPC and MIL-101 (Cr) NPs in the structure of Zn-MOF NPC@ MIL nanohybrid.

Fig. 2B displays the XRD spectrum of Zn-MOF NPC, MIL-101 (Cr), and Zn-MOF NPC@MIL nanohybrid samples. The main diffraction peaks 9.8° and 24.8° confirm the successful synthesis of MOF-5 crystalline phases.

According to the XRD of the Zn-MOF NPC sample, after the calcination process, the impurity diffraction peaks have been removed, which indicates that the carbon material has been completely converted. As a result of the carbonization process, ZnO was reduced by carbon and then evaporated at 900 °C, and the residue was removed by acid washing (Ma et al., 2016). Two the broad peaks at  $2\theta = 25^\circ$  (002) and  $44^\circ$  (100) assigned to graphitic carbon, which confirm the amorphous of the Zn-MOF NPC (Ong et al., 2019; Kumar et al., 2011). Also, crystal planes 8.78°, 18.98°, and 23.71° of MIL-101 and Zn-MOF NPC@MIL samples have obvious adsorption peaks in the region of  $2\theta = 220, 511, \text{ and } 852$  (Liu et al., 2021). The XRD patterns were in perfect agreement with MIL-

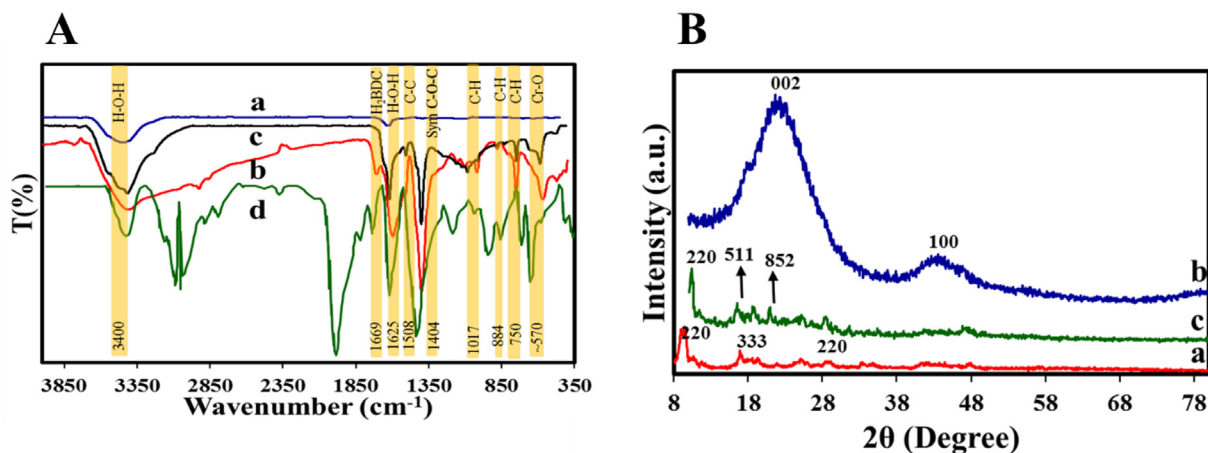


**Fig. 2.** A) FT-IR spectrum of a) Zn-MOF NPC, b) MIL-101 (Cr), c) Zn-MOF NPC@MIL nanohybrid, d) H<sub>2</sub>BDC; B) XRD patterns of a) Zn-MOF NPC, b) MIL-101 (Cr), c) Zn-MOF NPC@MIL nanohybrid.

101 (Cr) the previously reported XRD results, so it could be a strong reason for the formation of adsorbents.

The morphology of the nanoadsorbents was determined using SEM images at various magnifications (Fig. 3A-D). Based on these images, the morphology of Zn-MOF NPC has a cubic structure similar to the original structure of Zn-MOF-5 (Bakhtiari and Azizian, 2018). Therefore, it can be observed that the carbonization process does not change the morphology of the precursor at 900 °C. On the other hand, it was observed that MIL-101 (Cr) NPs have a polyhedral (octahedral) crystal texture in agreement with previous reports (Fig. 3C) (Hong et al., 2009; Noorpoor et al., 2017). Furthermore, there was no evidence of the presence of any needle-shaped crystals representative of unreacted H<sub>2</sub>BDC, indicating the success of supplementary purification processes. Also, the HF modulator has caused uniformity and an increase in the average size of the crystalline particles (Ren et al., 2014). SEM images of Zn-MOF NPC@MIL nanohybrid (Fig. 3D) show irregular surfaces, which confirm the proper synthesis of the final nanohybrid. Fig. 5A shows the particle size distribution (PSD) of Zn-MOF NPC@MIL nanohybrid obtained from images SEM. For this purpose, about 50 particles of the particles in the image have been measured. As can be seen, the most frequent particle size is 200–250 nm, which is due to the presence of macromolecules of Zn-MOF NPC.

The mapping images (Fig. 3E) show the uniform distribution of C, N, O, Cr, and Zn elements on the surface of the Zn-MOF NPC@MIL nanohybrid. Comparing the EDX peaks of the elements showed that the Cr peaks have a weaker intensity than C, N, O, and Zn due to the low percentage of Cr in the nanohybrid structure.

The TEM images (Fig. 4) clearly illustrate that MIL-101 (Cr) NPs were dispersed homogeneously on the Zn-MOF NPC.

The textural properties and BET specific surface area of pure MIL-101 (Cr) NPs, Zn-MOF NPC, and Zn-MOF NPC@MIL nanohybrid were investigated using nitrogen adsorption analysis. Table 2 and Fig. 6 show the results of BET and Barrett-Joyner-Halenda (BJH). These figures show that the adsorption of N<sub>2</sub> on all prepared sorbents was acceptably reversible with obvious hysteresis loop at P/P<sub>0</sub> > 0.5. The formation of hysteresis loops at high relative pressures refers to the dominance of mesopores over micropores and macropores in adsorbents. As can be seen from the graphs (Fig. 5B), the MIL-101 (Cr) NPs show type I isotherm, that confirm the microporous nature of the synthesized NPs. The Zn-MOF NPC, and Zn-MOF NPC@MIL nanohybrid exhibit type IV isotherm with a hysteresis loop, which is related to their mesoporous structure. This type of hysteresis loop is related to materials with the following conditions (Bakhtiari and Azizian, 2018):

- i) the ratio of the macropore area to the total surface area is very low.
- ii) the ratio of the micropore volume to the total pore volume is average.

The comparison between the prepared Zn-MOF NPC@MIL nanohybrid with pure Zn-MOF NPC, representation that the textural properties of the synthesized Zn-MOF NPC@MIL nanohybrid were significantly improved compared to pure Zn-MOF NPC. The BET specific surface areas of the prepared samples MIL-101 (Cr), Zn-MOF NPC, and Zn-MOF NPC@MIL nanohybrid were estimated to be 3440.2, 893.71, and 1331.8 m<sup>2</sup> g<sup>-1</sup>, respectively. Therefore, the hybrid Zn-MOF NPC with a small percentage of MIL-101 (Cr) NPs has a significantly increased surface area. It is inferred that the remarkable adsorption efficiency of this nanohybrid is attributed to its high surface area, the more surface-active sites, and the remarkable pore volume. The other important parameter related to the porosity of prepared adsorbents is BJH-plot (see Table 2 and Fig. 6b). As can be observed, this value to MIL-101 (Cr), Zn-MOF NPC, and Zn-MOF NPC@MIL nanohybrid was found to be 0.503, 1.33, 1.147 cm<sup>3</sup> g<sup>-1</sup>, respectively. On the other hand, this result confirms a reduction in total pore volume and pore diameter than that of pure Zn-MOF NPC. Based on the IUPAC classification, pore diameters are divided into three categories: micropore (the pore size < 2 nm), mesopore (the pore size 2–50 nm), and macropore (the pore size > 50) (Chen et al., 2010; Sharafinia et al., 2023; Bouzari et al., 2021; Babaei et al., 2020). Since the diameter pores of the synthesized Zn-MOF NPC@MIL nanohybrid is between 2 and 50 nm, it has a mesoporous structure, which is in agreement with the results of BJH-plot (Fig. 5C).

Thermogravimetric analysis (TGA) (with a heating rate of 10 °C/min and temperature to 800 °C) was used to investigate the thermal stability of Zn-MOF NPC, MIL-101 (Cr), and Zn-MOF NPC@MIL nanohybrid synthesized. Three samples showed excellent thermal stability (Fig. 5D). The observed TGA curve of Zn-MOF NPC showed similar thermal behavior with other previous reports (Fig. 5D-a). As the Fig. 5D-a shows, the main mass loss due to carbonization occurs about 400 °C. The initial weight losses < 150 °C in the Fig. 5D-b were related to the decomposition of organic solvent and the evaporation of residual adsorbed water. The second stage of reduction is related to the decomposition of H<sub>2</sub>BDC bonds, which occurs at 200 °C and is then fully carbonized at a higher temperature (Fig. 5D-b). Also, according to Fig. 5D-c, the main stage of nanohybrid decomposition takes place at temperatures >400 °C, therefore can be said that Zn-MOF NPC@MIL nanohybrid is a thermal stable adsorbent.

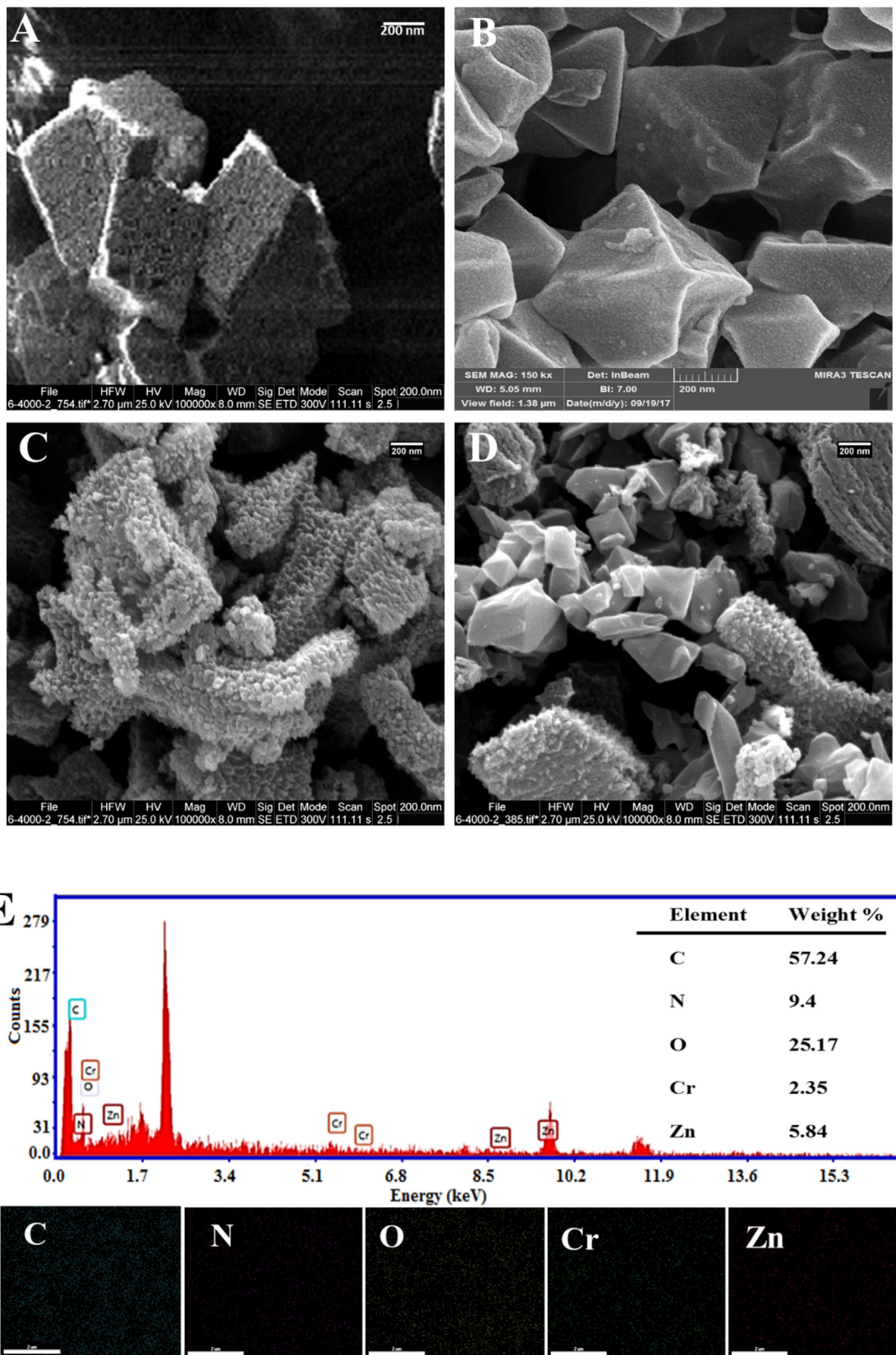


Fig. 3. SEM image of A) Zn-MOF, B) MIL-101 (Cr) NPs, C) Zn-MOF NPC, D) Zn-MOF NPC@ MIL nanohybrid; E) Elemental mapping and EDX of Zn-MOF NPC@ MIL nanohybrid.

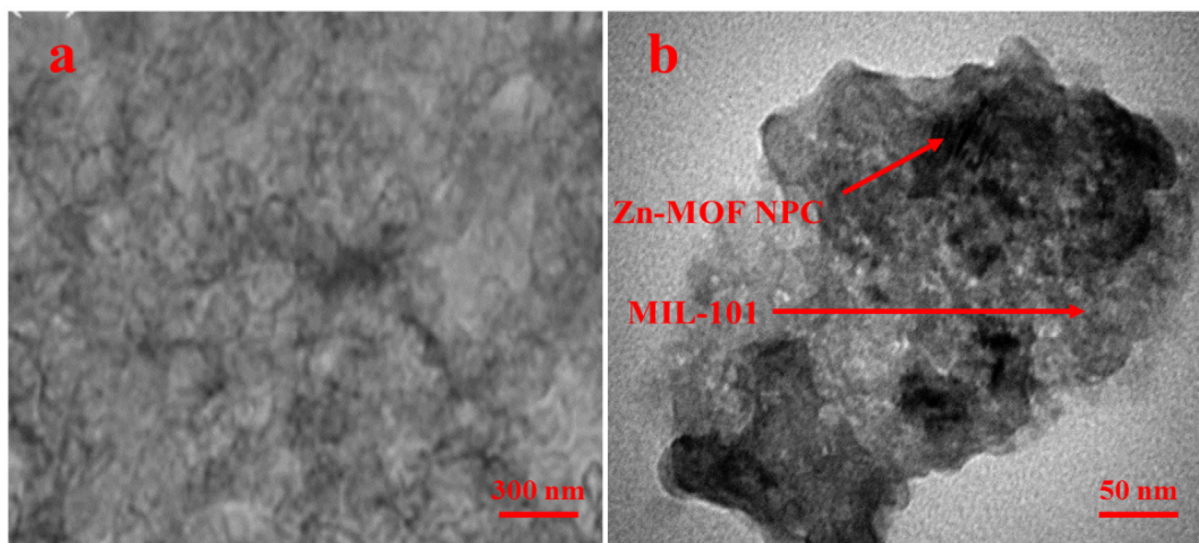


Fig. 4. The TEM image a) Zn-MOF NPC and b) Zn-MOF NPC@ MIL nanohybrid.

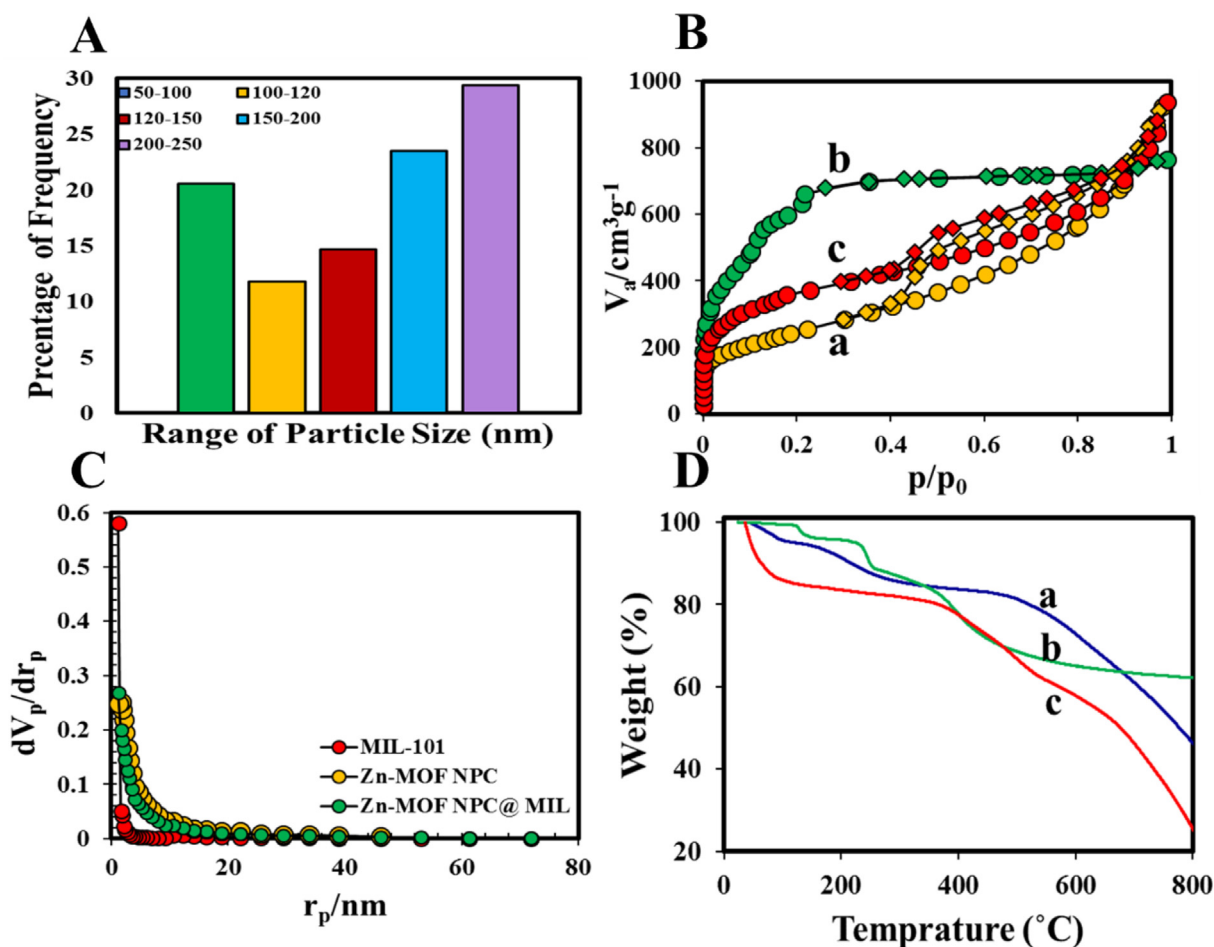
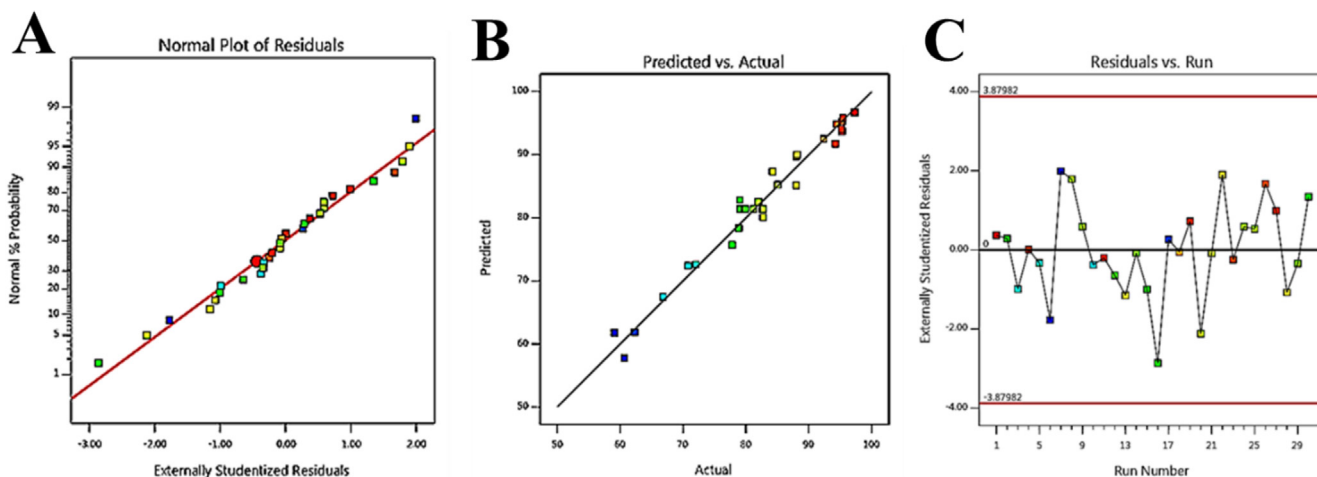


Fig. 5. A) PSD curves of Zn-MOF NPC@MIL nanohybrid; B) a)  $N_2$  Adsorption/ desorption isotherms of a) Zn-MOF NPC, b) MIL-101 (Cr), c) Zn-MOF NPC@MIL nanohybrid; C) BJH- plot of the samples; D) TGA curves of a) Zn-MOF NPC, b) MIL-101 (Cr), c) Zn-MOF NPC@MIL nanohybrid.

Table 2  
Porous structure parameters of MIL-101 (Cr), Zn-MOF NPC, and Zn-MOF NPC@MIL nanohybrid.

Adsorbent	$S_{BET} / m^2/g$	Mean pore diameter/ nm	Pore volume $V_{BJH}$	$V_t / cm^3/g$
MIL-101 (Cr)	3440.2	1.375	0.503	1.182
Zn-MOF NPC	893.71	6.38	1.33	1.42
Zn-MOF NPC@MIL	1331.8	4.32	1.147	1.44



**Fig. 6.** A) The curve of the normal probability; B) the curve of the predicted response versus actual response; C) analysis of residual for the response to the Zn-MOF-5 NPC@MIL nanohybrid.

**Table 3**  
Independent variables and levels of the process for CCD-RSM.

Independent variables	Symbol	Levels of independent variables				
		$-\alpha$	-1	0	+1	$+\alpha$
Loading (Wt.%)	a	10	15	20	25	30
Concentration (mg. L <sup>-1</sup> )	b	20	50	80	110	140
pH	c	2	4	6	8	10
Tim (min)	d	20	30	40	50	60

**Table 4**  
Independent variables and levels of the process for CCRSM.

Run	a	b	c	d	Zn-MOF NPC@MIL nanohybrid	
					Re% (Actual)	Re% (Predicted)
1	30	80	6	40	98.56	97.95
2	10	80	6	40	80.11	79.63
3	20	80	10	40	72.05	73.65
4	15	50	4	50	96.53	96.52
5	15	110	4	50	73.31	73.86
6	15	110	8	50	60.36	63.03
7	20	140	6	40	61.92	59
8	20	80	2	40	84.01	81.32
9	20	80	6	40	84.01	82.64
10	15	110	8	30	68.11	68.73
11	25	50	4	50	96.74	97.08
12	20	80	6	40	81.15	82.64
13	20	20	6	40	89.45	91.28
14	20	80	6	40	82.45	82.64
15	20	80	6	40	80.37	82.64
16	25	110	4	30	80.3	84.08
17	15	110	4	30	63.57	63.13
18	20	80	6	60	93.62	93.71
19	20	80	6	20	96.48	95.3
20	15	50	4	30	85.51	88.58
21	25	110	8	30	86.35	86.49
22	15	50	8	50	89.25	86.44
23	25	50	8	30	95.7	96.11
24	20	80	6	40	84.01	82.64
25	20	80	6	40	83.88	82.64
26	25	50	4	30	95.49	92.95
27	15	50	8	30	96.53	94.94
28	25	110	4	50	89.28	91
29	25	50	8	50	83.23	83.8
30	25	110	8	50	79.07	76.97

#### 4. Experiment design with central composite response surface methodology (RSM-CCD)

Response surface methodology (RSM) is a software and multi-variate experimental modeling technique. This method is employed to study the relationship between several parameters simultaneously, reduce the number of experiments, and optimize experimental processes (Gholamiyan et al., 2020). RSM-CCD is one of the RSM methods used in the field of analytical spectrum (de Oliveira et al., 2006), chromatography (Stafiej et al., 2006); electroanalysis (Rudd et al., 2016), and adsorption (Jain et al., 2011; Kiran and Thanasekaran, 2011; Özdemir et al., 2011). In this research, Design Expert 11.0.3.0 and the RSM-CCD method were used to design the experiments. The response can be related to selected variables using quadratic models to the optimization of parameters. To illustrate the communication between MB adsorption efficiency and tested parameters, a quadratic equation model as used according to the equation following (Abbasi et al., 2020; El Hassani et al., 2017):

$$a_0 + \sum_{i=1}^k a_i X_i + \sum_{i=1}^k a_{ii} X_i^2 + \sum_{i=1}^k \sum_{j=1}^k a_{ij} X_i X_j + e_0 \quad (3)$$

**Table 5**

Model summary statistics for MB adsorption response by Zn-MOF NPC@MIL nanohybrid.

Zn-MOF NPC@MIL nanohybrid			
Source	Sequential p-value	Adjusted R <sup>2</sup>	Predicted R <sup>2</sup>
Linear	< 0.0001	0.59	0.45
2FI	0.04	0.70	0.64
Quadratic	< 0.0001	0.95	0.85
Cubic	0.05	0.98	0.81

**Table 6**

The ANOVA results of the response surface modified quadratic model.

Zn-MOF NPC@MIL nanohybrid			
		R <sup>2</sup>	
Std. Dev.	2.49		0.9822
Mean	82.46	Adjusted R <sup>2</sup>	0.95
C.V. %	3.2	Predicted R <sup>2</sup>	0.8563
PRESS	480.8	Adeq Precision	22.1219
-2 Log Likelihood	119.07	BIC	170.09
		AICc	183.36

**Table 7**

Analysis of variance for the modified quadratic.

Zn-MOF NPC@MIL nanohybrid					
Source	Sum of Squares	df	Mean Square	F-value	p-value
<b>Model</b>	3253.86	14	232.42	37.49	< 0.0001
a-Loading	503.02	1	503.02	81.14	< 0.0001
b-Concentration	1563.37	1	1563.37	252.19	< 0.0001
c-pH	88.32	1	88.32	14.25	0.0018
d-time	3.77	1	3.77	0.6087	0.4447
ab	274.90	1	274.90	44.34	< 0.0001
ac	10.23	1	10.23	1.65	0.2184
ad	14.51	1	14.54	2.35	0.1465
bc	0.5644	1	0.5644	0.0910	0.7670
bd	7.80	1	7.80	1.26	0.2797
cd	270.22	1	270.22	43.59	< 0.0001
a <sup>2</sup>	64.76	1	64.76	10.45	0.0056
b <sup>2</sup>	96.49	1	96.49	15.57	< 0.0013
c <sup>2</sup>	45.61	1	45.61	7.36	0.0161
d <sup>2</sup>	241.28	1	241.28	38.92	0.0001
<b>Residual</b>	92.99	15	6.20		
Lack of Fit	80.30	10	8.03	3.16	0.1077
Pure Error	12.69	5	2.54		
<b>Cor Total</b>	3346.85	29			

Also, multiple regression analysis equation is used to calculate coded variables (see Eq. 4) (Nam et al., 2018):

$$X_i = \frac{X_i - X_0}{\delta X} \quad (4)$$

which, y, a<sub>i</sub>, a<sub>ij</sub>, a<sub>ijj</sub>, X<sub>i</sub>, X<sub>0</sub>, and δX are the response variable, constant-coefficient, linear coefficient, quadratic coefficient, cross product coefficient (interaction coefficient), the independent variables, the real variables, and the step change values between low (-1) and high (+1) levels, respectively.

#### 4.1. Optimization of adsorption of MB onto Zn-MOF-5 NPC@MIL nanohybrid using CCD-RSM

30 runs by RSM-CCD were designed to investigate the effects of four main variables on MB adsorption efficiency by Zn-MOF NPC@MIL nanohybrid (Table 3). Table 4 shows the average experimental and predicted results. Also, to ensure the repeatability of the experiments and to prove the normal dispersion of the experimental data, the central point parameters are repeated six times.

#### 4.2. Analysis of variant (ANOVA)

For MB removal by Zn-MOF NPC@MIL nanohybrid, mean, linear, 2FI, quadratic and cubic models were studied, and it was observed that the quadratic model is the best model for the analysis of experimental data. R<sup>2</sup> is an essential parameter in investigating experimental responses. This value is 1, which confirms the high accuracy of the model (Biglarijoo et al., 2016). In addition, it suggested highly appropriate correlation between adjusted (0.95) and predicted (0.85) variables with R<sup>2</sup>, that this value confirms the fitting of existing data with new observations. In this work, this difference is minimal (<0.2) for the synthesized nanohybrid, so the model is highly accurate. Also, Fig. 8(b) shows a high correlation between the actual and predicted values.

The importance of each coefficient and the strength of interaction between each independent variable are determined by p-value and p-value, respectively. P-value is smaller than 0.05, and F-value must be greater than 1 so that the model parameters are acceptable (El Hassani et al., 2017). Based on ANOVA results for adsorption of MB by Zn-MOF NPC@MIL nanohybrid, a very low p-value (i.e. < 0.0001) and a large F-value confirm the significance of the model (see Table 5). As well as, the Lack of fit for the models was not significant comparative to the pure error. The

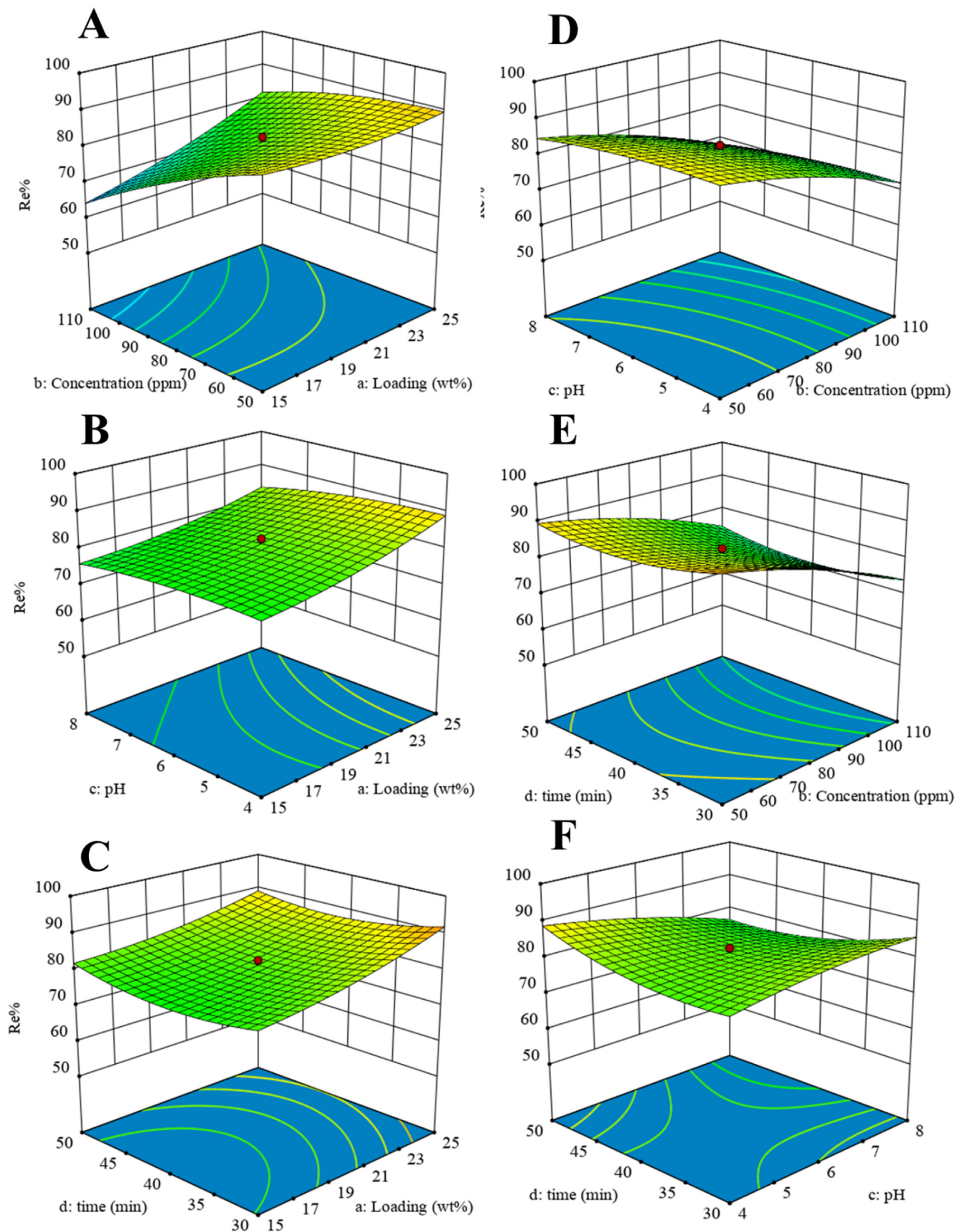


**Fig. 7.** Response surface graphs of MB adsorption onto Zn-MOF-5 NPC@MIL nanohybrid: **A)** the effect of loading and concentration, **B)** the effect of loading and pH, **C)** the effect of loading and time, **D)** the effect of concentration and pH, **E)** the effect of concentration and time, and **F)** the effect of time and pH.

codded, and actual Eqs for MB removal by Zn-MOF-5 NPC@MIL nano hybrid are indicated in Eqs. 5 and 6, respectively. (See Tables 6 and 7).

$$\begin{aligned} \text{Re}\% = & 81.39 + 4.58 * a - 8.07 * b - 1.92 * c - 0.3965 * d \\ & + 4.15 * ab - 4.11c * d + 1.58a^2 - 1.88b^2 - 1.29 \\ & + 2.97d^2 \end{aligned} \quad (5)$$

$$\begin{aligned} \text{Re}\% = & 133.904 - 3.75 \text{ Loading} \\ & - 0.49 \text{ Initial Concentration of MB} + 11.12 \text{ pH} \\ & - 1.17 \text{ time} + 0.027 \text{ Loading} \\ & * \text{ Initial Concentration of MB} - 0.205 \text{ pH} * \text{ time} \\ & + 0.061 \text{ Loading}^2 \\ & - 0.002(\text{Initial Concentration of MB})^2 - 0.32 \text{ pH}^2 \\ & + 0.029 \text{ time}^2 \end{aligned} \quad (6)$$

#### 4.3. Diagnostic model

The next method to investigate the correctness of the model proposed by the software is to study the normality of the data, which must have a normal distribution. Based on Fig. 6a, it can be said that this model has a normal distribution for the synthesized adsorbent. On the other hand, the proposed model reliability is confirmed in Fig. 6b (results of mathematical model and experimental data). The analysis of residuals is a powerful tool for diagnosing the proposed model and predicting the response (Abbasi et al., 2020). The residual equal distribution in the range of the adsorbed amount shows that it is of the order of magnitude of the variety of experimental results due to handling, and therefore the proposed model is acceptable and describes the adsorption process well (Fig. 6c).

#### 4.4. Response surface analysis to Zn-MOF-5 NPC@MIL nano hybrid

Fig. 7 shows the 3D graphs of the effects of the variables of MIL-101 (Cr) NPs loading percentage, initial concentration of MB, pH,

and time against the Re%. As can be seen, wt% (Fig. 7A, B, and C) and time (Fig. 7C, E, and F) had less effect on other variables. As can be seen from Fig. 7A, H, and D, the effect of initial concentration on the Re% is much greater than the effect of time and pH, and with increasing initial concentration (50 mg/L), the Re% increases. After reaching the equilibrium point, the Re% is almost constant because at high concentrations the active sites are saturated, which leads to repulsion between the adsorbent and the dye molecules (Rotte et al., 2014). Fig. 7B, D, and C show the effect of pH on MB removal by Zn-MOF-5 NPC@MIL nano hybrid. The Re% of MB increases slightly with increasing pH. The highest Re% of MB was obtained at pH = 8, which related to the pHPzc of the nano hybrid (the pHPzc of the Zn-MOF-5 NPC@MIL nano hybrid was 4.4). At acidic pHs, the surface of the Zn-MOF-5 NPC@MIL nano hybrid has a more positive charge and thus has a lower Re%. The reduction of Re% in lower pH is related to the competition between MB cations and H<sup>+</sup> ions on the surface of the Zn-MOF-5 NPC@MIL nano hybrid. However, at basic pHs, the Re% of MB is higher due to the opposite charge of the nano hybrid surface and dye molecules (Fig. 8A) (Chandane and Singh, 2016).

#### 4.5. Optimization and validation

After adjusting the fitting model, the CCD-RSM optimization objective was used to define the optimal values of the independent variables to produce the ideal Re% of adsorption of MB. This software predicted that for Zn-MOF-5 NPC@MIL nano hybrid Re% is 95.7 under optimal conditions reported in Table 8:

**Table 8**

The optimal amount for adsorption of MB by Zn-MOF-5 NPC@MIL nano hybrid.

Symbol	The optimal values
a (Wt.%)	25
b (mg. L <sup>-1</sup> )	50
c	8
d (min)	30

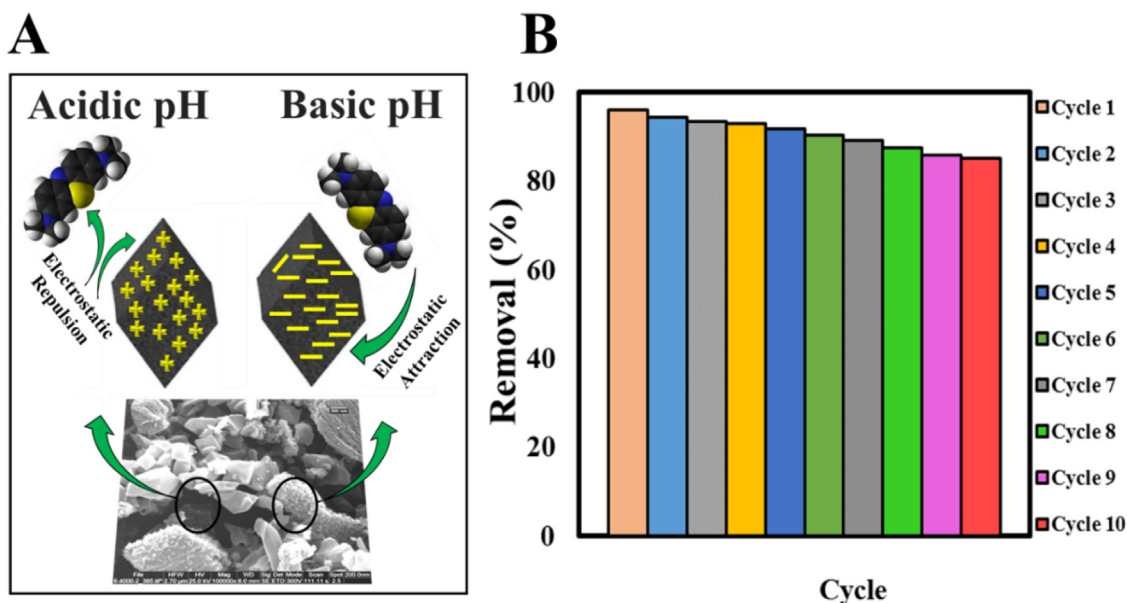


**Fig. 8.** A) Mechanism of MB adsorption by Zn-MOF-5 NPC@MIL nano hybrid at acidic and basic pHs, B) Reusability of Zn-MOF NPC@MIL nano hybrid by adsorption-desorption process for ten consecutive cycles.

## 5. Adsorption isotherm

Four famous isotherms of Langmuir (Langmuir, 1916) (Fig. 9A), Freundlich (Freundlich, 1907); Temkin, and Dubinin Radushkevitch (D-R) (Temkin and Pyzhev, 1940), were used to study experimental data, which their linear forms are shown in Table S1:

Table S2 exhibited the isotherms constant values. Since the  $R^2$  value of the Langmuir isotherm is higher than the other three isotherms, this isotherm is most consistent with the experimental data. The adsorption of MB molecules takes place on the surfaces of nanohybrid which is heterogeneous, and the adsorbed MB molecules were interacting with each other according to the Freundlich model.

## 6. Study of the effect of contact time and kinetic MB removal

The kinetics models of the pseudo-first-order (PFO) (Lagergren and Svenska) (Lagergren, 1898), pseudo-second-order (PSO) (Ho and McKay) (Lagergren, 1898); Elovich (Elovich and Larinov) (Ghasemian Lemraski et al., 2021), and intraparticle diffusion to the investigating of the kinetic data were used. Table S3 shows the linear form of each kinetic Eqs.

According to the results reported in Table S4, PSO kinetic model (Fig. 9B) was able to well describe the experimental data obtained for the adsorption of MB by Zn-MOF-5 NPC@MIL nanohybrid. Fig. 9a shows the good linear relation between time (t) and  $t/q_t$ .

Also, the possible mechanism of MB uptake includes the following steps (Fig. 9C) (Baghdadi et al., 2016):

Step 1: bulk diffusion.

Step 2: film diffusion.

Step 3: pore diffusion or intraparticle diffusion.

Step 4: adsorption of MB on the adsorbent surface.

## 7. Adsorption thermodynamics

The effect of temperature on the adsorption of MB was examined using thermodynamic studies. Eqs. 7 and 8 were used to calculate  $\ln K_c$  and the changes of Gibbs free energy, respectively (Baghdadi et al., 2016):

$$\ln K^{\circ} = \frac{qe}{C_e} \quad (7)$$

$$\Delta G^{\circ} = -RT \ln K^{\circ} \quad (8)$$

In this Eqs.  $K^{\circ}$ , T (K) and R (8.314 J. mol<sup>-1</sup> K<sup>-1</sup>) are the equilibrium constant, temperature, and the universal gas constant, respectively (Table 9). The achieved amounts of  $\Delta G^{\circ}$  to all used adsorbents here are negative, which confirms the adsorption of MB by them is spontaneous. The standard entropy changes ( $\Delta S^{\circ}$ ) and enthalpy changes ( $\Delta H^{\circ}$ ) for the adsorption process, were obtained from the slope and intercept  $\ln K^{\circ}$  versus  $1/T$  graph (i.e. Van't Hoff Eq.) (Fig. 9D) (Baghdadi et al., 2016), respectively.

$$\ln K^{\circ} = \frac{\Delta S^{\circ}}{R} - \frac{\Delta H^{\circ}}{RT} \quad (9)$$

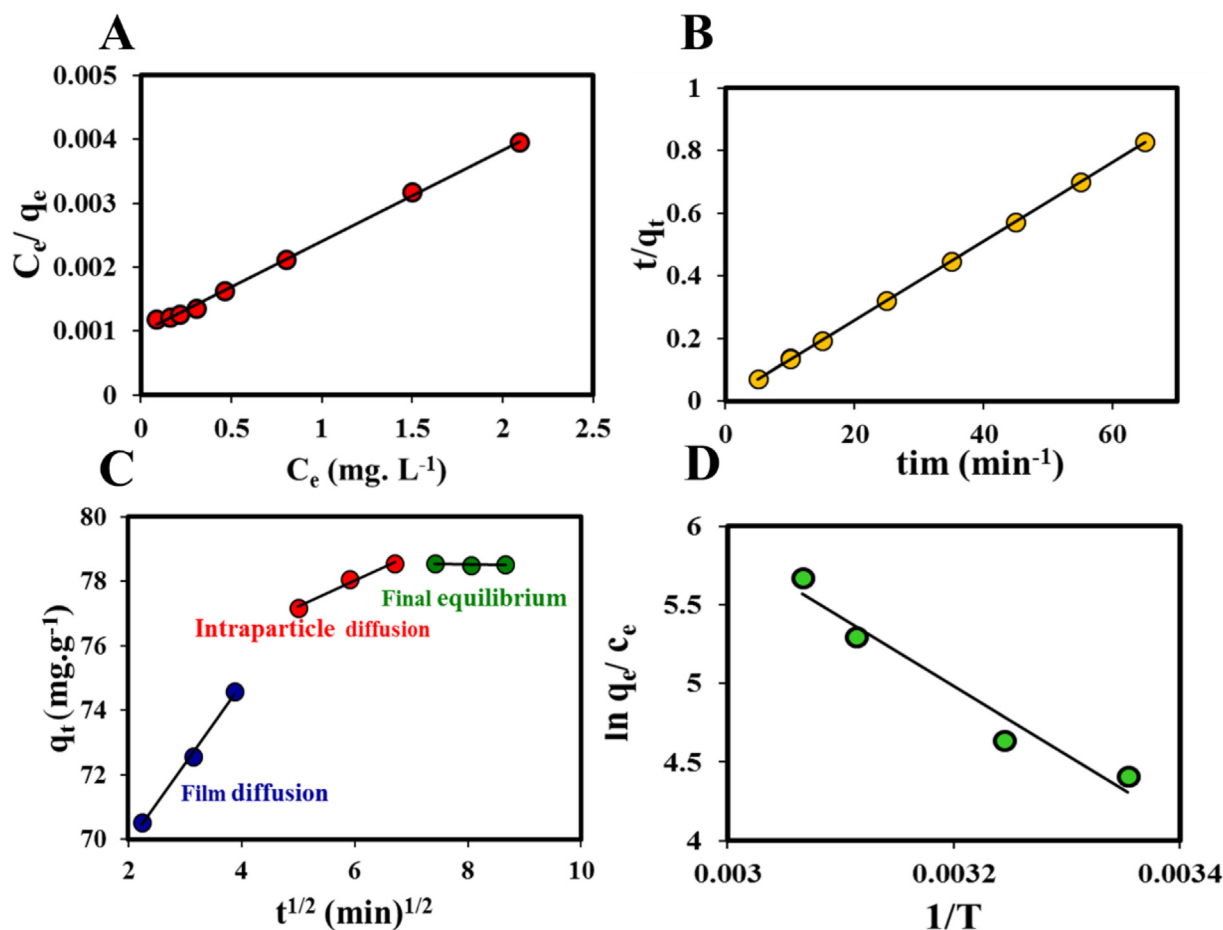


Fig. 9. A) The plot of  $\frac{C_e}{q_e}$  vs  $C_e$ , B) The plot of time and  $t/q_t$ , C) Three steps of the intraparticle diffusion model, D) The graph of the  $\ln q_e/C_e$  versus  $1/T$  for MB adsorption onto Zn-MOF-5 NPC@MIL nanohybrid.

**Table 9**

Thermodynamic parameters for MB removal onto Zn-MOF-5 NPC@MIL nanohybrid.

Adsorbent	Parameter	Temperature			
		298.15	308.15	321.15	326.15
Zn-MOF-5 NPC@MIL nanohybrid	K <sup>c</sup>	4.41	4.63	5.29	5.67
	$\Delta G^\circ$ (Kj.mol <sup>-1</sup> )	-10.939	-11.886	-14.148	-15.388
	$\Delta H^\circ$ (Kj.mol <sup>-1</sup> )	-0.520			
	$\Delta S^\circ$ (Kj.mol <sup>-1</sup> )	2.26			

**Table 10**Comparison of the maximum adsorption capacity ( $Q_m$ ) of Zn-MOF-5 NPC@MIL nanohybrid found in the literature for MB removal.

Sorbent	$Q_m$ (mg.g <sup>-1</sup> )	Ref.
Zn-MOF-5 NPC@MIL nanohybrid	<b>1000</b>	<b>Present work</b>
SDS/RM	89.471	(Efome et al., 2018)
CO <sub>2</sub> neutralized activated red mud	9.768	(Sahu et al., 2015)
Fe <sub>3</sub> O <sub>4</sub> NPs-SDS	769.23	(Gopakumar et al., 2017)
Magnetic Cymopolia barbata biomass	192.2	(Gopakumar et al., 2019)
Magnetic Sargassum horneri biomass	144.4	(Angelova et al., 2016)
NaOH-treated rice husk	37.97	(Chowdhury et al., 2011)

According to the results, the value of  $\Delta H^\circ$  to the adsorption of MB onto Zn-MOF-5 NPC@MIL nanohybrid is negative (exothermic) and positive (endothermic), respectively (Bedin et al., 2016). On the other hand, the reduction of the absolute value of  $\Delta G^\circ$  with temperature indicates a lower tendency for the adsorption of MB on the nanohybrid used at higher temperatures.

## 8. Comparison of the $q_m$ of Zn-MOF-5 NPC@MIL nanohybrid of this work with other adsorbents

In this study, a very inexpensive adsorbent with easy and rapid synthesis was used to remove MB. The results showed a significant amount of  $q_m$  for removal of MB by Zn-MOF-5 NPC@MIL nanohybrid compared to other adsorbents in the literature (Table 10).

## 9. Investigation the reusability of the Zn-MOF-5 NPC@MIL nanohybrid

Reusability and stability of nanohybrid are two key parameters for the widespread use of adsorbents. Thus, the adsorption-desorption recycling used to study of the durability of the Zn-MOF-5 NPC@MIL nanohybrid (Fig. 8B). As Fig. 8B shows, this nanohybrid could be used for up to ten cycles without significantly reducing their performance. Therefore, higher, repeatability, durability and excellent stability of Zn-MOF-5 NPC@MIL nanohybrid indicate the suitability of this adsorbent to remove contaminants.

## 10. Conclusion

The removal of MB dye from wastewater was investigated by Zn-MOF NPC@MIL nanohybrid and it was observed that this nanoadsorbent has an excellent adsorption capacity to remove this dye. RSM-CCD was used to optimize four parameters: loading percentage MIL-101 (Cr) NPs, initial concentration of MB, contact time and pH parameters. The results of study showed that it follows the quadratic model. Also, the study of adsorption isotherm and kinetics shows that the Langmuir isotherm model and PSO kinetics successfully describe the equilibrium adsorption data. Investigation of

thermodynamics of adsorption showed that adsorption of MB by Zn-MOF NPC@MIL nanohybrid is spontaneous and exothermic under optimal experimental conditions. Therefore, this research shows that the synthesized nanohybrid can be considered as a new and excellent adsorbent due to its high adsorption capacity and short equilibrium time.

## Declaration of Competing Interest

The authors declare that they have no known competing financial interests or personal relationships that could have appeared to influence the work reported in this paper.

## Acknowledgments

The authors are thankful for the financial support accepted by the research councils of the Nanotechnology Research Center, Research Institute of Petroleum Industry.

## Appendix A. Supplementary material

Supplementary data to this article can be found online at <https://doi.org/10.1016/j.arabjc.2023.105288>.

## References

- Abbasi, Z., Farrokhnia, A., Garcia-Lopez, E.I., Zargar Shoushtari, M., Aghaie, E., 2020. Synthesis of ZnO-Ag 2 CO 3-Fe 3 O 4@ rGO core-shell structure: magnetically separable photocatalyst for degradation of MB using the Box-Behnken design. *Journal of Materials Science: Materials in Electronics* 31, 19554–19568.
- Abney, C.W., Gilhula, J.C., Lu, K., Lin, W., 2014. Metal-organic framework templated inorganic sorbents for rapid and efficient extraction of heavy metals. *Advanced Materials* 26 (47), 7993–7997.
- Ahmadpour, A., Do, D.D., 1996. The preparation of active carbons from coal by chemical and physical activation. *Carbon* 34 (4), 471–479.
- Angelova, R., Baldikova, E., Pospiskova, K., Maderova, Z., Safarikova, M., Safarik, I., 2016. Magnetically modified Sargassum horneri biomass as an adsorbent for organic dye removal. *Journal of Cleaner Production* 137, 189–194.
- Azizian, S., 2004. Kinetic models of sorption: a theoretical analysis. *Journal of colloid and Interface Science* 276 (1), 47–52.
- Babaei, B., Bezaatpour, A., Amiri, M., Szunerits, S., Boukherroub, R., 2018. Magnetically Reusable MnFe2O4 Nanoparticles Modified with Oxo-Peroxo Mo (VI) Schiff-Base Complexes: A High Efficiency Catalyst for Olefin Epoxidation under Solvent-Free Conditions. *ChemistrySelect* 3 (10), 2877–2881.
- Babaei, B., Bezaatpour, A., Basharnavaz, H., 2020. Robust and fast oxidation of sulfides by immobilized Mo (VI) complex on magnetic nanoparticles in solvent-free condition. *Polyhedron* 179, 114382.
- Baghdadi, M., Ghaffari, E., Aminzadeh, B., 2016. Removal of carbamazepine from municipal wastewater effluent using optimally synthesized magnetic activated carbon: adsorption and sedimentation kinetic studies. *Journal of environmental chemical engineering* 4 (3), 3309–3321.
- Baghdadi, M., Ghaffari, E., Aminzadeh, B., 2016. Removal of carbamazepine from municipal wastewater effluent using optimally synthesized magnetic activated carbon: adsorption and sedimentation kinetic studies. *Journal of environmental chemical engineering* 4 (3), 3309–3321.
- Bakhtiar, N., Azizian, S., 2018. Nanoporous carbon derived from MOF-5: a superadsorbent for copper ions. *ACS omega* 3 (12), 16954–16959.
- Bedin, K.C., Martins, A.C., Cazetta, A.L., Pezoti, O., Almeida, V.C., 2016. KOH-activated carbon prepared from sucrose spherical carbon: Adsorption equilibrium, kinetic and thermodynamic studies for Methylene Blue removal. *Chemical Engineering Journal* 286, 476–484.
- Bezaatpour, A., Askarizadeh, E., Akbarpour, S., Amiria, M., Babaei, B., 2017. Green oxidation of sulfides in solvent-free condition by reusable novel Mo (VI)

- complex anchored on magnetite as a high-efficiency nanocatalyst with eco-friendly aqueous H<sub>2</sub>O<sub>2</sub>. *Molecular Catalysis* 436, 199–209.
- Biglarijoo, N., Mirbagheri, S.A., Ehteshami, M., Ghaznavi, S.M., 2016. Optimization of Fenton process using response surface methodology and analytic hierarchy process for landfill leachate treatment. *Process Safety and Environmental Protection* 104, 150–160.
- Bouzari, N., Bezaatpour, A., Babaei, B., Amiri, M., Boukherroub, R., Szunerits, S., 2021. Modification of MnFe<sub>2</sub>O<sub>4</sub> surface by Mo (VI) pyridylimine complex as an efficient nanocatalyst for (ep) oxidation of alkenes and sulfides. *Journal of Molecular Liquids* 330, 115690.
- Cabello, C.P., Picó, M.F.F., Maya, F., del Rio, M., Palomino, G.T., 2018. UiO-66 derived etched carbon/polymer membranes: High-performance supports for the extraction of organic pollutants from water. *Chemical Engineering Journal* 346, 85–93.
- Chandane, V., & Singh, V. K. (2016). Adsorption of safranin dye from aqueous solutions using a low-cost agro-waste material soybean hull. *Desalination and Water Treatment*, 57(9), 4122–4134. V. Chandane, V.J.D. Singh, W. Treatment, 57 (2016) 4122–4134.
- Chang, L., Li, J., Duan, X., Liu, W., 2015. Porous carbon derived from Metal-organic framework (MOF) for capacitive deionization electrode. *Electrochimica Acta* 176, 956–964.
- Chen, S., Zhang, J., Zhang, C., Yue, Q., Li, Y., Li, C., 2010. Equilibrium and kinetic studies of methyl orange and methyl violet adsorption on activated carbon derived from Phragmites australis. *Desalination* 252 (1–3), 149–156.
- Chen, G., Hai, J., Wang, H., Liu, W., Chen, F., Wang, B., 2017. Gold nanoparticles and the corresponding filter membrane as chemosensors and adsorbents for dual signal amplification detection and fast removal of mercury (II). *Nanoscale* 9 (9), 3315–3321.
- Chowdhury, S., Mishra, R., Saha, P., Kushwaha, P., 2011. Adsorption thermodynamics, kinetics and isosteric heat of adsorption of malachite green onto chemically modified rice husk. *Desalination* 265 (1–3), 159–168.
- de Oliveira, F. S., & Korn, M. (2006). Spectrophotometric determination of sulphate in automotive fuel ethanol by sequential injection analysis using dimethylsulphonazo (III) reaction. *Talanta*, 68(3), 992–999. F.S. de Oliveira, M.J. T. Korn, 68 (2006) 992–999.
- Efome, J. E., Rana, D., Matsuura, T., & Lan, C. Q. (2018). Metal-organic frameworks supported on nanofibers to remove heavy metals. *Journal of Materials Chemistry A*, 6(10), 4550–4555. J.E. Efome, D. Rana, T. Matsuura, C.Q.J.J.o.M.C.A. Lan, 6 (2018) 4550–4555.
- Farha, O. K., & Hupp, J. T. (2010). Rational design, synthesis, purification, and activation of metal-organic framework materials. *Accounts of chemical research*, 43(8), 1166–1175. O.K. Farha, J.T.J.A.o.c.r. Hupp, 43 (2010) 1166–1175.
- Farha, O. K., Özgür Yazaydın, A., Eryazici, I., Malliakas, C. D., Hauser, B. G., Kanatzidis, M. G., ... & Hupp, J. T. (2010). De novo synthesis of a metal-organic framework material featuring ultrahigh surface area and gas storage capacities. *Nature chemistry*, 2(11), 944–948.
- Férey, G., Mellot-Draznieks, C., Serre, C., Millange, F., Dutour, J., Surblé, S., & Margiolaki, I. (2005). A chromium terephthalate-based solid with unusually large pore volumes and surface area. *Science*, 309(5743), 2040–2042.
- Freundlich, H. (1907). Über die adsorption in lösungen. *Zeitschrift für physikalische Chemie*, 57(1), 385–470. H.J.Z.f.p.C. Freundlich, 57 (1907) 385–470.
- El Hassani, K., Beakou, B.H., Kalnina, D., Oukani, E., Anouar, A., 2017. Effect of morphological properties of layered double hydroxides on adsorption of azo dye Methyl Orange: A comparative study. *Applied Clay Science* 140, 124–131.
- Gholamiyan, S., Hamzehloo, M., Farokhnia, A., 2020. RSM optimized adsorptive removal of erythromycin using magnetic activated carbon: Adsorption isotherm, kinetic modeling and thermodynamic studies. *Sustainable Chemistry and Pharmacy* 17, 10030.
- Gopakumar, D.A., Pasquini, D., Henrique, M.A., De Morais, Grohens, Y., Thomas, S., 2017. Meldrum's acid modified cellulose nanofiber-based polyvinylidene fluoride microfiltration membrane for dye water treatment and nanoparticle removal. *ACS Sustainable Chemistry & Engineering* 5 (2), 2026–2033.
- Gopakumar, D.A., Arumukhan, V., Gelamo, R.V., Pasquini, D., de Morais, Rizal, S., Khalil, H.A., 2019. Carbon dioxide plasma treated PVDF electrospun membrane for the removal of crystal violet dyes and iron oxide nanoparticles from water. *Nano-Structures & Nano-Objects* 18, 10026.
- Hong, D.Y., Hwang, Y.K., Serre, C., Férey, G., Chang, J.S., 2009. Porous chromium terephthalate MIL-101 with coordinatively unsaturated sites: surface functionalization, encapsulation, sorption and catalysis. *Advanced Functional Materials* 19 (10), 1537–1552.
- Horcajada, P., Chalati, T., Serre, C., Gillet, B., Sebrie, C., Baati, T., ... Gref, R., 2010. Porous metal-organic-framework nanoscale carriers as a potential platform for drug delivery and imaging. *Nature materials* 9 (2), 172–178.
- Jiao, C., Wang, Y., Li, M., Wu, Q., Wang, C., & Wang, Z. (2016). Synthesis of magnetic nanoporous carbon from metal-organic framework for the fast removal of organic dye from aqueous solution. *Journal of Magnetism and Magnetic Materials*, 407, 24–30. C. Jiao, Y. Wang, M. Li, Q. Wu, C. Wang, Z.J.J.o.M. Wang, M. Materials, 407 (2016) 24–30.
- Journet, C., Maser, W. K., Bernier, P., Loiseau, A., de La Chapelle, M. L., Lefrant, D. S., ... & Fischer, J. E. (1997). Large-scale production of single-walled carbon nanotubes by the electric-arc technique. *nature*, 388(6644), 756–758.
- Kaneti, Y. V., Tang, J., Salunkhe, R. R., Jiang, X., Yu, A., Wu, K. C. W., & Yamauchi, Y. (2017). Nanoarchitected design of porous materials and nanocomposites from metal-organic frameworks. *Advanced materials*, 29(12), 1604898.
- Jain, M., Garg, V.K., Kadirvelu, K., 2011. Investigation of Cr (VI) adsorption onto chemically treated Helianthus annuus: optimization using response surface methodology. *Bioresource technology* 102 (2), 600–605.
- Kiran, B., & Thanasekaran, K. (2011). Copper biosorption on Lyngbya putealis: application of response surface methodology (RSM). *International Biodegradation & Biodegradation*, 65(6), 840–845. Kiran, B., Thanasekaran, K.J.I. B., 2011. Biodegradation 65, 840–845.
- Kong, D., Wang, N., Qiao, N., Wang, Q., Wang, Z., Zhou, Z., & Ren, Z. (2017). Facile preparation of ion-imprinted chitosan microspheres enwrapping Fe<sub>3</sub>O<sub>4</sub> and graphene oxide by inverse suspension cross-linking for highly selective removal of copper (II). *ACS Sustainable Chemistry & Engineering*, 5(8), 7401–7409.
- Kumar, S., Dory, Y. L., Lepage, M., & Zhao, Y. (2011). Surface-grafted stimuli-responsive block copolymer brushes for the thermo-, photo- and pH-sensitive release of dye molecules. *Macromolecules*, 44(18), 7385–7393. S. Kumar, Y.L. Dory, M. Lepage, Y.J.M. Zhao, 44 (2011) 7385–7393.
- Lagergren, S. K. (1898). About the theory of so-called adsorption of soluble substances. *Sven. Vetenskapsakad. Handlingar*, 24, 1–39. S.K.v.H. Lagergren, 24 (1898) 1–39.
- Chasemian Lemraski, E., Jahangirian, H., Dashti, M., Khajehali, E., Sharafinia, S., Rafiee-Moghaddam, R., & Webster, T. J. (2021). Antimicrobial double-layer wound dressing based on chitosan/polyvinyl alcohol/copper: in vitro and in vivo assessment. *International journal of nanomedicine*, 223–235.
- Li, B., Wen, H. M., Zhou, W., & Chen, B. (2014). Porous metal-organic frameworks for gas storage and separation: what, how, and why?. *The journal of physical chemistry letters*, 5(20), 3468–3479.
- Li, X., Yuan, H., Quan, X., Chen, S., & You, S. (2018). Effective adsorption of sulfamethoxazole, bisphenol A and methyl orange on nanoporous carbon derived from metal-organic frameworks. *Journal of Environmental Sciences*, 63, 250–259. X. Li, H. Yuan, X. Quan, S. Chen, S.J.J.o.E.S. You, 63 (2018) 250–259.
- Lin, K. Y. A., & Chen, B. C. (2016). Efficient elimination of caffeine from water using Oxone activated by a magnetic and recyclable cobalt/carbon nanocomposite derived from ZIF-67. *Dalton Transactions*, 45(8), 3541–3551. K.-Y.A. Lin, B.-C.J.D.T. Chen, 45 (2016) 3541–3551.
- Langmuir, I., 1916. The constitution and fundamental properties of solids and liquids. Part I. Solids. *Journal of the American chemical society* 38 (11), 2221–2295.
- Liu, F., Chung, S., Oh, G., & Seo, T. S. (2012). Three-dimensional graphene oxide nanostructure for fast and efficient water-soluble dye removal. *ACS Appl Mater Interfaces* 4: 922–927. Liu, F., Chung, S., Oh, G., Seo, T.S., 2012. ACS Appl. Mater. Interfaces 4, 922–927.
- Liu, B., Shioyama, H., Jiang, H., Zhang, X., & Xu, Q. (2010). Metal-organic framework (MOF) as a template for syntheses of nanoporous carbons as electrode materials for supercapacitor. *Carbon*, 48(2), 456–463.
- Liu, Z., He, W., Zhang, Q., Shapour, H., & Bakhtari, M. F. (2021). Preparation of a GO/MIL-101 (Fe) composite for the removal of methyl orange from aqueous solution. *ACS omega*, 6(7), 4597–4608. Z. Liu, W. He, Q. Zhang, H. Shapour, M.F.J. A.o. Bakhtari, 6 (2021) 4597–4608.
- Liu, L., Gao, Z. Y., Su, X. P., Chen, X., Jiang, L., & Yao, J. M. (2015). Adsorption removal of dyes from single and binary solutions using a cellulose-based bioadsorbent. *ACS Sustainable Chemistry & Engineering*, 3(3), 432–442. Liu, L., Gao, Z.Y., Su, X.P., Chen, X., Jiang, L., Yao, J.M., 2015. ACS Sustain. Chem. Eng. 3, 432–442.
- Liu, X., Yan, L., Yin, W., Zhou, L., Tian, G., Shi, J., ... & Zhao, Y. (2014). A magnetic graphene hybrid functionalized with beta-cyclodextrins for fast and efficient removal of organic dyes. *Journal of Materials Chemistry A*, 2(31), 12296–12303.
- Luo, X., Lei, X., Cai, N., Xie, X., Xue, Y., & Yu, F. (2016). Removal of heavy metal ions from water by magnetic cellulose-based beads with embedded chemically modified magnetite nanoparticles and activated carbon. *ACS Sustainable Chemistry & Engineering*, 4(7), 3960–3969.
- Ma, X., Li, L., Wang, S., Lu, M., Li, H., Ma, W., & Keener, T. C. (2016). Ammonia-treated porous carbon derived from ZIF-8 for enhanced CO<sub>2</sub> adsorption. *Applied Surface Science*, 369, 390–397. X. Ma, L. Li, S. Wang, M. Lu, H. Li, W. Ma, T.C.J.A.S.S. Keener, 369 (2016) 390–397.
- Ma, X., Li, L., Chen, R., Wang, C., Li, H., & Wang, S. (2018). Heteroatom-doped nanoporous carbon derived from MOF-5 for CO<sub>2</sub> capture. *Applied Surface Science*, 435, 494–502.
- Macdonald, J.E., Veinot, J.G., 2008. Removal of residual metal catalysts with iron/iron oxide nanoparticles from coordinating environments. *Langmuir* 24 (14), 7169–7177.
- Marpaung, F., Kim, M., Khan, J. H., Konstantinov, K., Yamauchi, Y., Hossain, M. S. A., ... & Kim, J. (2019). Metal-organic framework (MOF)-derived nanoporous carbon materials. *Chemistry—An Asian Journal*, 14(9), 1331–1343. F. Marpaung, M. Kim, J. H. Khan, K. Konstantinov, Y. Yamauchi, M.S.A. Hossain, J. Na, J.J.C.A.A.J. Kim, 14 (2019) 1331–1343.
- Nam, S. N., Cho, H., Han, J., Her, N., & Yoon, J. (2018). Photocatalytic degradation of aceulfame K: optimization using the Box-Behnken design (BBD). *Process Safety and Environmental Protection*, 113, 10–21. S.-N. Nam, H. Cho, J. Han, N. Her, J.J.P.S. Yoon, E. Protection, 113 (2018) 10–21.
- Noorpoor, Z., Pakdehi, S. G., & Rashidi, A. (2017). High capacity and energy-efficient dehydration of liquid fuel 2-dimethyl amino ethyl azide (DMAZ) over chromium terephthalic (MIL-101) nanoadsorbent. *Adsorption*, 23, 743–752. Z. Noorpoor, S.G. Pakdehi, A.J.A. Rashidi, 23 (2017) 743–752.
- O'Keeffe, M., & Yaghi, O. M. (2012). Deconstructing the crystal structures of metal-organic frameworks and related materials into their underlying nets. *Chemical reviews*, 112(2), 675–702. M. O'Keeffe, O.M.J.C.r. Yaghi, 112 (2012) 675–702.

- Ong, C., Shi, Y., Chang, J., Alduraie, F., Ahmed, Z., & Wang, P. (2019). Polydopamine as a versatile adhesive layer for robust fabrication of smart surface with switchable wettability for effective oil/water separation. *Industrial & Engineering Chemistry Research*, 58(12), 4838–4843. Ong, C., Shi, Y., Chang, J., Alduraie, F., Ahmed, Z., Wang, P., 2019. E.C. Research 58, 4838–4843.
- Özdemir, E., Duranoğlu, D., Beker, Ü., & Avcı, A. Ö. (2011). Process optimization for Cr (VI) adsorption onto activated carbons by experimental design. *Chemical Engineering Journal*, 172(1), 207–218. E. Özdemir, D. Duranoğlu, Ü. Beker, A.Ö.J.C. E.J. Avcı, 172 (2011) 207–218.
- Rahmaninia, A., Mansoori, Y., Nasiri, F., Bezaatpour, A., & Babaei, B. (2019). Surface decorated magnetite nanoparticles with birhodanine and MoO<sub>2</sub>Cl<sub>2</sub> (dmf) 2 as a new magnetic catalyst for epoxidation of olefins. *Journal of Particle Science and Technology*, 5(1), 47–60.
- Ren, J., Musyoka, N. M., Langmi, H. W., Segakweng, T., North, B. C., Mathe, M., & Kang, X. (2014). Modulated synthesis of chromium-based metal-organic framework (MIL-101) with enhanced hydrogen uptake. *International Journal of Hydrogen Energy*, 39(23), 12018–12023. J. Ren, N.M. Musyoka, H.W. Langmi, T. Segakweng, B.C. North, M. Mathe, X.J.i.o.h.e. Kang, 39 (2014) 12018–12023.
- Rotte, N. K., Yerramala, S., Boniface, J., & Srikanth, V. V. (2014). Equilibrium and kinetics of Safranin O dye adsorption on MgO decked multi-layered graphene. *Chemical Engineering Journal*, 258, 412–419. K. Rotte, S. Yerramala, J. Boniface, V.V.J.C.E.J. Srikanth, 258 (2014) 412–419.
- Rudd, N. D., Wang, H., Fuentes-Fernandez, E. M., Teat, S. J., Chen, F., Hall, G., ... & Li, J. (2016). Highly efficient luminescent metal-organic framework for the simultaneous detection and removal of heavy metals from water. *ACS applied materials & interfaces*, 8(44), 30294–30303.
- Sahu, M. K., Sahu, U. K., & Patel, R. K. (2015). Adsorption of safranin-O dye on CO 2 neutralized activated red mud waste: process modelling, analysis and optimization using statistical design. *RSC Advances*, 5(53), 42294–42304.
- Salehi, S., & Hosseini, M. (2021). Evaluation of CO<sub>2</sub> and CH<sub>4</sub> adsorption using a novel amine modified MIL-101-derived nanoporous carbon/polysaccharides nanocomposites: Isotherms and thermodynamics. *Chemical Engineering Journal*, 410, 128315. S. Salehi, M.J.C.E.J. Hosseini, 410 (2021) 128315.
- Salunkhe, R. R., Young, C., Tang, J., Takei, T., Ide, Y., Kobayashi, N., & Yamauchi, Y. (2016). A high-performance supercapacitor cell based on ZIF-8-derived nanoporous carbon using an organic electrolyte. *Chemical Communications*, 52(26), 4764–4767. R.R. Salunkhe, C. Young, J. Tang, T. Takei, Y. Ide, N. Kobayashi, Y. J.C.C. Yamauchi, 52 (2016) 4764–4767.
- Seenivasan, R., Chang, W. J., & Gunasekaran, S. (2015). Highly sensitive detection and removal of lead ions in water using cysteine-functionalized graphene oxide/polypyrrole nanocomposite film electrode. *ACS applied materials & interfaces*, 7(29), 15935–15943.
- Sharafinia, S., Rashidi, A., Babaei, B., & Orooji, Y. (2023). Nanoporous carbons based on coordinate organic polymers as an efficient and eco-friendly nano-sorbent for adsorption of phenol from wastewater. *Scientific Reports*, 13(1), 13127. Sharafinia, S., Rashidi, A., Babaei, B., Orooji, Y., 2023. Sci. Rep. 13, 13127.
- Stafiej, A., Pyrzyńska, K., Ranz, A., & Lankmayr, E. (2006). Screening and optimization of derivatization in heating block for the determination of aliphatic aldehydes by HPLC. *Journal of biochemical and biophysical methods*, 69(1-2), 15–24.
- Tanhaei, B., Ayati, A., Sillanpää, M., 2019. Magnetic xanthate modified chitosan as an emerging adsorbent for cationic azo dyes removal: Kinetic, thermodynamic and isothermal studies. *International journal of biological macromolecules* 121, 1126–1134.
- Szczęśniak, B., Choma, J., & Jaroniec, M. (2018). Gas adsorption properties of hybrid graphene-MOF materials. *Journal of colloid and interface science*, 514, 801–813. B. Szczeniak, J. Choma, M.J.J.o.c. Jaroniec, i. science, 514 (2018) 801–813.
- Temkin, M., & Pyzhev, V. (1940). Kinetics of the synthesis of ammonia on promoted iron catalysts. *Acta Physicochim*, 12(1), 217–222. M. Temkin, V. Pyzhev, (1940).
- Torad, N. L., Hu, M., Kamachi, Y., Takai, K., Imura, M., Naito, M., & Yamauchi, Y. (2013). Facile synthesis of nanoporous carbons with controlled particle sizes by direct carbonization of monodispersed ZIF-8 crystals. *Chemical communications*, 49(25), 2521–2523.
- Wang, Y., Tong, Y., Xu, X., & Zhang, L. (2018). Metal-organic framework-derived three-dimensional porous graphitic octahedron carbon cages-encapsulated copper nanoparticles hybrids as highly efficient enrichment material for simultaneous determination of four fluoroquinolones. *Journal of Chromatography A*, 1533, 1–9. Y. Wang, Y. Tong, X. Xu, L.J.J.o.C.A. Zhang, 1533 (2018) 1–9.
- Wang, X., Wang, Y., Hou, H., Wang, J., & Hao, C. (2017). Ultrasonic method to synthesize glucan-g-poly (acrylic acid)/sodium lignosulfonate hydrogels and studies of their adsorption of Cu<sup>2+</sup> from aqueous solution. *ACS Sustainable Chemistry & Engineering*, 5(8), 6438–6446. Wang, X., Wang, Y., Hou, H., Wang, J., Hao, C.J.A.S.C., 2017. Engineering 5, 6438–6446.
- XXu, L., Huang, X., Ma, J., Huang, J., Fan, Y., Li, H., ... & Huang, W. (2017). Value of three-dimensional strain parameters for predicting left ventricular remodeling after ST-elevation myocardial infarction. *The international journal of cardiovascular imaging*, 33, 663–673.
- Xu, Y., Bao, J., Zhang, X., Li, W., Xie, Y., Sun, S., ... & Zhao, C. (2019). Functionalized polyethersulfone nanofibrous membranes with ultra-high adsorption capacity for organic dyes by one-step electrospinning. *Journal of colloid and interface science*, 533, 526–538. Xu, Y., Bao, J., Zhang, X., Li, W., Xie, Y., Sun, S., Zhao, W., Zhao, C., 2019. J. Colloid Interface Sci. 533, 526–538.
- Yagub, M. T., Sen, T. K., Afroze, S., & Ang, H. M. (2014). Dye and its removal from aqueous solution by adsorption: a review. *Advances in colloid and interface science*, 209, 172–184. M.T. Yagub, T.K. Sen, S. Afroze, H.M.J.A.i.c. Ang, i. science, 209 (2014) 172–184.
- Yang, Xu, W., Tomita, A., & Kyotani, T. (2005). The template synthesis of double coaxial carbon nanotubes with nitrogen-doped and boron-doped multiwalls. *Journal of the American Chemical Society*, 127(25), 8956–8957. Q. Yang, W. Xu, A. Tomita, T.J.J.o.t.A.C.S. Kyotani, 127 (2005) 8956–8957.
- Yuan, D., Chen, J., Tan, S., Xia, N., & Liu, Y. (2009). Worm-like mesoporous carbon synthesized from metal-organic coordination polymers for supercapacitors. *Electrochemistry communications*, 11(6), 1191–1194. D. Yuan, J. Chen, S. Tan, N. Xia, Y.J.E.c. Liu, 11 (2009) 1191–1194.
- Zhang, S., Zhou, Y., Nie, W., Song, L., & Zhang, T. (2012). Preparation of uniform magnetic chitosan microcapsules and their application in adsorbing copper ion (II) and chromium ion (III). *Industrial & engineering chemistry research*, 51(43), 14099–14106. S. Zhang, Y. Zhou, W. Nie, L. Song, T.J.I. Zhang, e.c. research, 51 (2012) 14099–14106.
- Zhao, Z., Wang, Y., Li, M., & Yang, R. (2015). High performance N-doped porous activated carbon based on chicken feather for supercapacitors and CO<sub>2</sub> capture. *RSC Advances*, 5(44), 34803–34811.
- Zhou, S., Shang, Q., Ji, J., & Luan, Y. (2021). A nanoplatfrom to amplify apoptosis-to-pyoptosis immunotherapy via immunomodulation of myeloid-derived suppressor cells. *ACS Applied Materials & Interfaces*, 13(40), 47407–47417. Zhou, S., Shang, Q., Ji, J., Luan, Y.J.A.A.M., 2021. Interfaces 13, 47407–47417.